

# Spectral distortion of cosmic background radiation by scattering on hot electrons. Exact calculations.

A.D. Dolgov<sup>1</sup>, S.H. Hansen

*INFN section of Ferrara  
Via del Paradiso 12, 44100 Ferrara, Italy*

dolgov@fe.infn.it, sthansen@fe.infn.it

S. Pastor<sup>2</sup>, D.V. Semikoz<sup>3</sup>

*Max-Planck-Institut für Physik (Werner-Heisenberg-Institut)  
Föhringer Ring 6, 80805 München, Germany*

pastor@mppmu.mpg.de, semikoz@mppmu.mpg.de

## ABSTRACT

The spectral distortion of the cosmic background radiation produced by the inverse Compton scattering on hot electrons in clusters of galaxies (thermal Sunyaev–Zel’dovich effect) is calculated for arbitrary optical depth and electron temperature. The distortion is found by a numerical solution of the exact Boltzmann equation for the photon distribution function. In the limit of small optical depth and low electron temperature our results confirm the previous analyses. In the opposite limits, our method is the only one that permits to make accurate calculations.

*Subject headings:* cosmic microwave background — cosmology: theory — galaxies: clusters: general — methods: numerical — scattering

## 1. Introduction

The frequency spectrum of the Cosmic Microwave Background Radiation (CMBR) is known to have the equilibrium black body form (in natural units in which  $\hbar = c = k_B = 1$ )

$$f_0(p_\gamma) = [\exp(p_\gamma/T_\gamma) - 1]^{-1}, \quad (1)$$

---

<sup>1</sup>ITEP, Bol. Cheremushkinskaya 25, Moscow 117259, Russia

<sup>2</sup>SISSA–ISAS and INFN section of Trieste, Via Beirut 2-4, 34014 Trieste, Italy

<sup>3</sup>Institute of Nuclear Research of the Russian Academy of Sciences, 60th October Anniversary Prospect 7a, Moscow 117312, Russia

with the temperature  $T_\gamma = 2.725 \pm 0.002$  K (Mather et al. 1999). No deviation from this perfect Planck distribution is observed with the accuracy of  $10^{-4}$ . These data present a strong evidence in support of Big-Bang cosmology. It is established that the cosmic plasma in the early universe was in a thermal equilibrium state and the spectrum remained practically undisturbed to the present epoch. Nevertheless, small deviations from the perfect Planck spectrum are possible, and they could provide interesting information about physical processes in the early universe that might take place at relatively small red-shifts,  $z \leq 10^7$ . At higher red-shifts all distortions of the thermal equilibrium spectrum would be efficiently smoothed down by the Compton scattering,  $\gamma + e \leftrightarrow \gamma + e$  and by the inelastic photon producing reactions, double Compton,  $\gamma + e \leftrightarrow 2\gamma + e$  or Bremsstrahlung,  $e + A \leftrightarrow e + A + \gamma$ . The first elastic process restores kinetic equilibrium, i.e. it forces the photon distribution function,  $f_\gamma$ , to take the Bose-Einstein form with a possible non-zero chemical potential,  $\mu$ , while the other two reactions push  $\mu$  down to zero.

There are several possible sources and mechanisms that could give rise to spectral distortions of the CMBR both in the early and the present day universe. In the early universe there could be electromagnetic decays of long-lived particles with life-time larger than  $\sim 100$  sec, in particular,  $\nu_H \rightarrow \nu_L + \gamma$ . A study of a possible distortion of the CMBR spectrum permits to obtain strong bounds on the probability of such decays (for a review, see Raffelt (1996)). In the present-day universe a very interesting spectral distortion can be induced by the scattering of cosmic background radiation on hot electrons in galactic clusters, known as the Sunyaev-Zel'dovich (SZ) effect (Zeldovich & Sunyaev 1969a,b; Sunyaev & Zeldovich 1970a,b). Observations of such a distortion, combined with those of thermal X-ray emission of the cluster gas, could help to extract important astrophysical information, in particular to measure the Hubble constant, or to study the evolution of clusters (for reviews see Zeldovich & Novikov (1983); Sunyaev & Zeldovich (1981); Rephaeli (1995a); Birkinshaw (1999a), and the updates in Birkinshaw (1999b) and Rephaeli (1999)).

Compton scattering conserves the number of photons, which implies that the SZ effect produces a systematic shift of photons from the low-energy part to the Wien side of the Planckian CMBR spectrum. To calculate the corresponding distortion of the spectral distribution one should use the Boltzmann kinetic equation for the distribution function of photons,  $f_\gamma$ ,

$$\frac{df_\gamma}{dt} = I_{coll} + S, \tag{2}$$

with properly taken collision integral  $I_{coll}$  and a possible source term,  $S$ .

In the early universe case one has to solve the system of such two coupled equations for the photon and electron/positron distributions. In the lowest order in the fine-structure constant,  $\alpha \simeq 1/137$ , only Compton and Coulomb scattering need to be taken into account. They have cross-sections of the order  $\alpha^2$ , while inelastic reactions contribute at most to the order  $\alpha^3$ . Because of technical difficulties this problem was treated only approximately especially for relativistic electrons. In the non-relativistic case the problem can be reduced to the partial differential equation describing diffusion in photon momentum space. For the particular case of Compton scattering such a reduction was done in 1957 by Kompaneets (Kompaneets 1957) and for inelastic processes

(double Compton scattering and Bremsstrahlung) by Lightman (Lightman 1981). Solutions to these equations in cosmological situations were analyzed in Bernstein & Dodelson (1990) and Hu & Silk (1993).

In the case of scattering of the CMB radiation on hot electrons in galactic clusters (thermal SZ effect) the Kompaneets equation has the form

$$\frac{\partial f_\gamma(X, t)}{\partial t} = n_e \sigma_T \frac{T_e}{m} \frac{\partial}{X^2 \partial X} \left[ X^4 \left( \frac{\partial f_\gamma}{\partial X} + \frac{T_\gamma}{T_e} f_\gamma (1 + f_\gamma) \right) \right], \quad (3)$$

where  $T_e$  and  $T_\gamma$  are the electron and photon temperatures,  $m$  is the electron mass,

$$X = \frac{p_\gamma}{T_\gamma} \quad (4)$$

is the dimensionless photon momentum,  $n_e$  is the electron number density, and  $\sigma_T = 8\pi\alpha^2/3m^2 = 6.65 \times 10^{-25} \text{ cm}^2$  is the Thomson cross-section. However, the electrons in the clusters are hot, with temperatures that can be larger than 15 keV, which means that the energy change of Compton scattered photons is not small enough to be accurately described by the Kompaneets equation.

There are basically two different approaches in the literature to extend the validity of this equation. In ref. Rephaeli (1995b) the relativistic form of the Maxwell velocity distribution of electrons is used and the frequency redistribution through Compton scattering is calculated (see also Wright (1979); Rephaeli & Yankovitch (1997); Sazonov & Sunyaev (1998); Molnar & Birkinshaw (1999)); this method is also known as the Radiative Transfer Approach. On the other hand, one can obtain a relativistic generalization of the Kompaneets equation, by expanding in series of the parameter  $\theta_e \equiv T_e/m$ . Low orders of this expansion were considered in the papers Stebbins (1997) and Challinor & Lasenby (1998), while Itoh et al. (1998) took into account relativistic corrections up to  $\mathcal{O}(\theta_e^5)$ . These two different methods are essentially consistent.

It has, however, been pointed out (Challinor & Lasenby 1998) that these results are not guaranteed to be accurate because the series approximation to the solution of the Boltzmann kinetic equation involves expansions in parameters which are not small. In particular it was recognized that the convergence is slow and possibly even asymptotic (for instance, to calculate the crossover frequency, where the thermal distortion vanishes, it is better to use a linear approximation in  $\theta_e$  than the expansion up to  $\mathcal{O}(\theta_e^3)$  or  $\mathcal{O}(\theta_e^5)$ ). In view of that it is desirable to solve the original kinetic equation (2) directly without any specific approximation. This problem was partly addressed in Itoh et al. (1998, 2000a) where the collision integral was numerically calculated for the unperturbed photon distribution eq. (1). This integral determines the first time derivative of the distribution function  $f_\gamma(X, 0)$  and in the limit of a small optical depth,

$$\tau = \int dl n_e \sigma_T \ll 1, \quad (5)$$

(the integral is taken along the line of sight through the cluster) gives the solution,  $f_\gamma(X, \tau) \approx f_0 + \tau I_{coll}[f_\gamma(X, 0)]$ . In a subsequent paper (Itoh et al. 2000b), the second order corrections

in  $\tau$  were calculated as a series in  $\theta_e$ . The results show a good agreement with solutions of the generalized Kompaneets equation in the limit of small optical depth and low electron temperatures,  $\theta_e = T_e/m \lesssim 0.03$  (i.e.  $T_e \lesssim 15$  keV).

In this paper we present an accurate numerical solution of the exact Boltzmann kinetic equation for arbitrary optical depth and electron temperature. In the limit of small  $\tau$  and  $\theta_e$  our results confirm those of the previous papers, and in particular of Itoh et al. (1998, 2000b). However, the method presented here permits to solve the equation precisely for an arbitrary optical depth and any isotropic electron distribution function. We use essentially the same method as the one we have developed for the calculations of the spectral distortion of light (Dolgov et al. 1997, 1999a) or heavy (Dolgov et al. 1998, 1999b) neutrinos at Big Bang Nucleosynthesis. An essential point of the calculations is an analytical reduction of the exact collision integral down to two dimensions (Semikoz & Tkachev 1995, 1997). In the case of Compton scattering the problem is much more complicated because the squared amplitude of this process is not a simple polynomial function of particle momenta as was the case for weak interaction in the low energy limit.

A reduction of the collision integral down to one dimension in the direct reaction term and down to two dimensions in the inverse reaction term was done in Poutanen & Svensson (1996) for the case of Boltzmann statistics (see also the review Nagirner & Poutanen (1994) for a discussion and relevant references). The method of these works is somewhat different from ours because we specially use the procedure of the integration suitable for the quantum statistics case when the direct reaction term (as well as the inverse one) contains the product of the distribution functions not only in the initial state but also in the final state,  $f_1 f_2 (1 + f_3)(1 - f_4)$  (see eq. 9), that makes the reduction down to one dimension impossible in principle if all the functions are considered as unknown.

The paper is organized as follows. In the next rather technical section we present the reduction of the 9-dimensional collision integral down to a 2-dimensional one. In section 3 the numerical solution of the integro-differential Boltzmann equation is described. In section 4 our results are presented and discussed. Finally in section 5 we give the conclusions.

## 2. The Boltzmann equation

We consider the Boltzmann equation (2) for the distribution function of photons,  $f_\gamma$ , taking into account only Compton scattering process,

$$\gamma(P_1) + e(P_2) \leftrightarrow \gamma(P_3) + e(P_4). \quad (6)$$

where  $P_i = (E_i, \mathbf{p}_i)$  are the particle 4-momenta. In this case the source term in the kinetic equation is absent,  $S = 0$ , and we have

$$\frac{df_\gamma}{dt} = I_{coll}, \quad (7)$$

where the collision integral  $I_{coll}$  takes the form

$$I_{coll} = \frac{1}{2E_1} \int \prod_{i=2}^4 \left( \frac{d^3 p_i}{(2\pi)^3 2E_i} \right) (2\pi)^4 \delta^4(P_1 + P_2 - P_3 - P_4) |M|^2 F(1, 2, 3, 4), \quad (8)$$

with the statistical factor,  $F$ , given by

$$F = f_\gamma(p_3) f_e(p_4) [1 + f_\gamma(p_1)] [1 - f_e(p_2)] - f_\gamma(p_1) f_e(p_2) [1 + f_\gamma(p_3)] [1 - f_e(p_4)], \quad (9)$$

and  $|M|^2$  is the matrix element squared of the process in eq. (6)

$$\begin{aligned} |M|^2 = & 4e^4 \left\{ m^4 \left[ \frac{1}{(P_1 \cdot P_2)^2} - \frac{2}{(P_1 \cdot P_2)(P_1 \cdot P_4)} + \frac{1}{(P_1 \cdot P_4)^2} \right] \right. \\ & \left. + 2m^2 \left[ \frac{1}{(P_1 \cdot P_2)} - \frac{1}{(P_1 \cdot P_4)} \right] + \frac{(P_1 \cdot P_4)}{(P_1 \cdot P_2)} + \frac{(P_1 \cdot P_2)}{(P_1 \cdot P_4)} \right\}, \end{aligned} \quad (10)$$

where  $m$  is the electron mass.

The collision term in eq. (8) is in principle a 9-dimensional phase space integral, that can be analytically reduced to a sum of two-dimensional integrals. When one defines the terms  $I_k$  for  $k = 1, \dots, 7$ , corresponding to the 7 terms in eq. (10), each of them reduces to

$$I_k(p_1) = \frac{\alpha^2}{2\pi p_1^2} \int_0^\infty \frac{p_2 dp_2}{E_2} \int_0^S dp_3 F J_k(p_1, p_2, p_3), \quad (11)$$

where  $\alpha \simeq 1/137$  is the fine-structure constant and the maximum value  $S$  for the momentum  $p_3$  is discussed in appendix B. The expressions for the integrands  $J_k$  are listed in appendix A. Each of the two-dimensional integrals in eq. (11) can be found numerically, which permits to evaluate  $I_{coll}$  in eq. (8). The spectral distortion of  $f_\gamma$  is then found from the evolution of the Boltzmann equation, eq. (7) (see the next section for the computational details). An important issue, which we have taken into account, is the reduction of the integration region in eq. (11). When one imposes conservation of 3-momenta, and in particular the fact that none of the momenta can be larger than the sum of the others, i.e.  $p_i \leq p_a + p_b + p_c$ , the integration region can be divided into several sub-regions where the functions  $J_k$  take different values. See the Appendices for the technical details.

### 3. Numerical solution of the Boltzmann equation

We have found the spectral distortion of  $f_\gamma$  produced by the SZ effect from the numerical solution of the Boltzmann equation (7).

We measure all momenta in units of photon temperature. Accordingly, we use the dimensionless photon frequency  $X$  from eq. (4) and measure time in units of the optical depth,  $\tau$ , given by eq. (5). In order to calculate the integral over electron momenta we introduce the electron temperature as

$$X_e = \frac{p_e}{T_\gamma} = R_T \frac{p_e}{T_e}, \quad (12)$$

where

$$R_T = \frac{T_e}{T_\gamma}, \quad (13)$$

is the ratio of electron to photon temperatures. We assume that electrons are always in equilibrium with the distribution

$$f_e = \left( e^{(E_e - \mu_e)/T_e} + 1 \right)^{-1}, \quad (14)$$

where  $E_e = \sqrt{m^2 + p_e^2}$  is the electron energy and  $\mu_e$  is their chemical potential. In the present paper we make the simplifying assumption of Boltzmann statistics<sup>4</sup> for electrons ( $f_e \ll 1$ ) and express  $\mu_e$  through the number density of electrons.

The integration over electron momenta in the two-dimensional integral in eq. (11) should formally be taken from zero to infinity, but we integrate only to  $p_e^{\max}$ . We found that for small  $T_e < 10$  keV it is enough to take  $p_e^{\max} = m$ , and for larger electron temperature  $T_e \sim 50$  keV integration till  $p_e^{\max} = 3m$  is sufficient.

For the dimensionless photon frequency,  $X$ , we introduce a grid of  $N_{\text{grid}}$  points, logarithmically spaced in the interval  $X_{\text{low}} \leq X \leq X_{\text{hi}}$ . We use  $X_{\text{low}} = 10^{-4}$ , which is small enough to maintain a sufficiently high precision of the calculations.  $X_{\text{hi}}$  actually depends both on the electron temperature  $T_e$  and the final optical depth  $\tau_{\text{fin}}$ . For small electron temperatures  $T_e < 10$  keV it is enough to take  $X_{\text{hi}} = 100$ . For higher temperatures and large optical depth  $\tau > 1$  we need to use much higher values of  $X_{\text{hi}}$ , because photons multiple-scatter into large momentum modes. For example, for calculation with  $T_e = 20$  keV and  $\tau_{\text{fin}} = 20$  (see the next section) we use  $X_{\text{hi}} = 10000$ . As for the number of points in the grid,  $N_{\text{grid}}$ , we always checked that it is large enough to maintain the desired precision. Typically 1600 points grid was good enough for our purposes.

As initial condition for eq. (7) we used equilibrium photon distribution function eq. (1), which in terms of  $X$  has the simple form

$$f_0(X) = \frac{1}{e^X - 1}. \quad (15)$$

For calculation of the two-dimensional integrals in eq. (11) we use the Gaussian quadratures method, see Press et al. (1992). For the evolution in "time",  $\tau$ , we use the simple Euler method, which is precise enough for the present calculations. Finally, for calculation of the photon distribution function in points between the grid points we used interpolation not in  $f_\gamma$  but in  $f_\gamma - f_0$  to perform 2D-integration. This trick strongly reduces numerical errors, coming from interpolation in the regions where the distribution of photons is close to the equilibrium one (i.e. for  $\tau < 1$ ).

---

<sup>4</sup>Note that our method is valid for any isotropic  $f_e$ , not necessarily in equilibrium, but here we restrict ourselves to the case of a Boltzmann equilibrium distribution in order to investigate the thermal SZ effect.

Additional difficulties in the numerical calculations come from the region of small photon momenta,  $X < 0.1$ . In this region some parts of the integrands in eq. (11) behave like  $1/X^5$ , while the complete collision integral is proportional to  $1/X$  for small  $X$  (due to the singularity  $1/X$  in the distribution function eq. (15)). This leads to large numerical errors for small momenta. On the other hand, asymptotically for small  $X$  each part of the collision integral eq. (11) has either a constant value or  $1/X$ -behavior. Using this fact, we calculate the integrals numerically for grid points with momenta  $X > X_{\text{small}}$  and extrapolate into the region of smaller  $X$ . In the calculations we use  $0.01 \leq X_{\text{small}} \leq 0.1$ .

Different parts of the integration region contribute differently to the collision integral in eq. (11) (see appendix B for the definitions of the regions). The main contribution comes from the large regions  $C_2$  and  $D_2$ . The regions  $C_1$  and  $D_1$  can be taken into account, but they contribute on the level of 1% in the region of small  $X < 0.1$  and could be neglected for larger  $X$ . The main numerical error comes from a small part of the integration regions  $C$  and  $D$  around the line  $Q^2 = 0$ . These regions give numerical errors up to 10% of the value of the collision integral for small photon momenta. The nature of this small-momentum error was discussed above. The regions  $A$  and  $B$  give corrections to the collision integrals in the sixth digit and could be neglected.

The ratio of the electron and photon temperatures,  $R_T$  (13), is very large in hot clusters. The CMB temperature is  $T_\gamma \sim 10^{-4}$  eV, while the electron temperature is  $T_e \sim 10$  keV. Since both photon and electron momenta are involved in the same expressions in the collision integral we may lose precision by many orders of magnitude if we keep realistic values of  $R_T \sim 10^8$ . The energy conservation implies  $p_3 = p_1 + E_2 - E_4$ , and since  $E_2 \sim E_4 \sim m = 511$  keV, the difference should cancel up to 10 digits in order to give numbers of the order  $p_1 \sim p_3 \sim 10^{-4}$  eV, and even more precisely for low photon momenta,  $X < 1$ . This numerical problem is solved in the following way. We calculate the collision integral for much higher photon temperatures  $T_\gamma \sim 1$  keV, and then diminish the temperature until the collision integral stops varying with a further temperature decrease. We assume that at this value of  $T_\gamma^{\text{min}}$  the collision integral reaches its asymptotical value and therefore reproduces the result for  $T_\gamma \sim 10^{-4}$  eV. We found that already at  $T_\gamma = 50$  eV the collision integral reaches asymptotical values. In most calculations we used  $T_\gamma^{\text{min}} = 10$  eV. Let us note, that already for  $T_\gamma = 1$  eV the numerical errors discussed in this paragraph become important.

In conclusion, we control all numerical errors in the solution of the kinetic equation (7), and we also check the result testing the conservation of the photon number (see the end of section 4).

## 4. Results

The distortion of the photon spectrum is usually presented in the form

$$\Delta I(X, \tau) = X^3(f_\gamma(X, \tau) - f_0(X)) , \quad (16)$$

where  $f_\gamma(X, \tau)$  is the photon distribution function calculated from the kinetic equation (2) and  $f_0(X)$  is the initial equilibrium photon distribution (1).

Instead of solving the kinetic equation directly, one could for a small optical depth,  $\tau \ll 1$ , make the Taylor expansion in  $\tau$  of the collision integral

$$I_{coll}(X, \tau) \approx I_{coll}(X, 0) + \tau \frac{\partial I_{coll}}{\partial \tau}(X, 0) + \mathcal{O}(\tau^2). \quad (17)$$

Then the distribution function  $f_\gamma(X, \tau)$  can be trivially found from eq. (7)

$$f_\gamma(X, \tau) \approx f_0(X) + \tau I_{coll}(X, 0) + \frac{\tau^2}{2} \frac{\partial I_{coll}}{\partial \tau}(X, 0) + \mathcal{O}(\tau^3), \quad (18)$$

and the spectral distortion takes the form

$$\Delta I(X, \tau) \approx \Delta I_1(X, \tau) + \Delta I_2(X, \tau) + \mathcal{O}(\tau^3), \quad (19)$$

where

$$\Delta I_1(X, \tau) = \tau X^3 I_{coll}(X, 0) \quad , \quad \Delta I_2(X, \tau) = \frac{\tau^2}{2} X^3 \frac{\partial I_{coll}}{\partial \tau}(X, 0) \quad (20)$$

The term  $\Delta I_1$  in eq. (20) corresponds to the single photon scattering. It requires only calculation of the collision integral with equilibrium distribution functions  $f_0(X)$ . Our calculation of the collision integral in this case agrees perfectly with the results obtained in Itoh et al. (1998, 2000a), as can be seen from fig. 1. In this figure we compare our numerical results for  $T_e = 10$  keV and  $T_e = 20$  keV with analytical fits from Itoh et al. (2000a).

The term  $\Delta I_2$  in eq. (20) is proportional to  $\tau^2$ , and it corresponds to the double photon scattering contributing to the spectral distortion. In order to calculate this term one can do the following: calculate  $I_{coll}(X, 0)$ , substitute the first two terms of the photon distribution function eq. (18) back into the collision integral and calculate all terms of order  $\tau$ . These terms correspond to the second term in eq. (17), which is responsible for the double photon scattering. In the paper Itoh et al. (2000b) this second order contribution to the spectral distortion was found approximately, up to the terms of the order  $\theta_e^2$ . By numerical integration of eq. (7) we have found the two-scattering contribution exactly from  $I_{coll}(X, \tau)$ .

In fig. 2 the double-scattering contribution into the spectral distortion as a function of dimensionless photon frequency  $X$  is presented for  $T_e = 10$  keV. The solid curve in fig. 2 is our exact result (up to small numerical errors). One could compare it with the series expansion in powers of  $\theta_e = T_e/m$  from Itoh et al. (2000b), which are shown by the dashed, short dashed and dotted lines (the definitions of functions  $Z_i$  are given in Itoh et al. (2000b)). As we can see from fig. 2, this expansion is in a good agreement with our result for relatively small  $X < 4$  and disagrees for a larger  $X$ . It demonstrates again (as the first-order terms in  $\tau$ ) a bad convergence of the expansion in terms of  $\theta_e$ .



In figure 3 we present the results for the spectral distortion of the CMB photons caused by the SZ effect for  $T_e = 20$  keV and the optical depth equal to one,  $\tau = 1$ . The dotted curve corresponds to the numerical solution of eq. (7). The solid line represents the single scattering contribution, namely the first term in eq. (19). The long dashed line corresponds to the double scattering contribution, namely the second term in eq. (19). The short dashed line is the sum of these two contributions. One can see from fig. 3 that even at optical depth  $\tau = 1$ , the spectral distortion is accurately described by the sum of single and double photon scatterings.

It should be noted that our results have been obtained with an initial isotropic photon distribution. This is an approximation of the real radiation distribution inside the clusters of galaxies, which are of finite extension. At the level of single scattering there is no problem since the radiation is isotropic prior to convolving with the Compton kernel. However the multiple scattering contributions to the spectral distortion could be affected by the geometrical properties of the cluster. For instance, Molnar & Birkinshaw (1999) used a Monte-Carlo method to take into account finite optical depth and bulk motion in a spherically symmetric uniform plasma. Therefore our results are exact in the case of an infinite medium.

For  $\tau \ll 1$ , the single scattering strongly dominates the spectral distortion, and in order to estimate the contribution of the second-order term, one should rescale the amplitude of the long dashed line in fig. 3 by the factor  $\tau$  and compare it with the solid line at any photon frequency  $X$ . In a realistic case one has  $\tau \leq 0.01$ , and the double scattering can be safely neglected everywhere, except for a small region in photon frequency  $X$  where the single scattering contribution vanishes.

The magnitude of the double photon scattering is demonstrated in figure 4 for the optical depth  $\tau = 0.01$ . The crossover frequency  $X_0$  (the photon frequency at which the distortion caused by the thermal SZ effect vanishes) is plotted as a function of the electron temperature (solid line). The regions around this line show the double scattering contribution to the spectral distortion. In the region between the dotted lines it is larger than 50%, between the short dashed lines it is larger than 10%, and between the long dashed lines it is larger than 1%.

When one calculates the distortion using the Kompaneets equation (3), the crossover frequency does not depend on the electron temperature, and it takes the constant value  $X_0 \simeq 3.83$ . The exact calculations show that the crossover frequency depends both on the electron temperature,  $\theta_e = T_e/m$  and the optical depth  $\tau$ . For small optical depths,  $0 < \tau < 0.05$ , a linear fit in  $\tau$  is very accurate

$$X_0 = \alpha(T_e) + \tau \beta(T_e), \quad (21)$$

and by doing such fits in the range,  $0 < \tau < 0.05$ , for many different electron temperatures one can find  $\alpha(T_e)$  and  $\beta(T_e)$  as functions of temperature

$$\alpha(T_e) \approx 3.830(1 + 1.162\theta_e - 0.8144\theta_e^2) \quad \text{and} \quad \beta(T_e) \approx 3.021\theta_e - 8.672\theta_e^2, \quad (22)$$

which fits better than  $4 \times 10^{-4}$  for  $0 < T_e < 50$  keV and  $0 < \tau < 0.05$ . The functional shape was chosen by simply looking at the corresponding graphs. By considering the graphs for  $\alpha(T_e)$

and  $\beta(T_e)$ , we have found no reason to include higher order terms. The fit parameters change only slightly for large optical depths,  $0.05 < \tau < 1$ . One can naturally perform similar fits for  $X_{\max}$  and  $X_{\min}$ , which are the dimensionless frequencies where the spectral distortion is maximal or minimal. We find

$$X_{\min} = 2.265 (1 - 0.0927 \theta_e + 2.38 \theta_e^2) + \tau (-0.00674 + 0.466 \theta_e) , \quad (23)$$

$$X_{\max} = 6.511 (1 + 2.41 \theta_e - 4.96 \theta_e^2) + \tau (0.0161 + 8.16 \theta_e - 35.9 \theta_e^2) . \quad (24)$$

We can compare these results with similar fits from the previous papers. For the interesting range of temperatures,  $0 < T_e < 50$  keV, and for negligible optical depth, we are in good agreement with the previous results (Birkinshaw 1999a; Challinor & Lasenby 1998; Itoh et al. 1998). In Molnar & Birkinshaw (1999) the fit in the optical depth is also made and for small  $\tau$  we are in good agreement. In this paper some of the effects of the cluster geometry were considered, which may explained why our results for larger  $\tau$  are somewhat different.

Finally in figure 5 the results for a large optical depth,  $\tau$ , are presented. The Taylor expansion in terms of  $\tau$ , eq. (19), is useless for  $\tau > 1$ , and the complete numerical solution of eq. (7) should be done. From figure 5 one can see that for  $\tau > 1$  the spectral distortion is dominated by multi-scattering contributions. Indeed, one and two-scattering contributions dominate the curves with  $\tau = 0.01$  and  $\tau = 1$ , and all distortion in these cases are in the region  $X < 20$ . Spectral distortion in higher modes come from multi-scattering contribution, demanding much larger optical depth.

Asymptotically for  $\tau \rightarrow \infty$  the photon distribution should reach the form

$$f_\gamma \rightarrow \left[ \exp \left( \frac{E - \mu}{T_e} \right) - 1 \right]^{-1} , \quad (25)$$

with the chemical potential  $\mu$  determined by the photon number conservation,  $\mu = T_e \log(\zeta(3)T_\gamma^3/T_e^3) \approx -1$  MeV (when  $T_\gamma \ll T_e$ ). However, even for  $\tau = 20$  the distribution is very far from the equilibrium one in eq. (25). A much larger  $\tau$  is necessary to equalize the temperatures of photons,  $T_\gamma = 2 \times 10^{-4}$  eV, and electrons,  $T_e \sim 20$  keV. We have estimated that one requires  $\tau \sim \sqrt{m/T_e} \ln(\rho_{fin}/\rho_{in})$ , where  $\rho_{in}$  and  $\rho_{fin}$  are the initial and final energy densities of photons. We have also calculated the same quantity numerically and found  $\tau \sim 250$  for  $T_e = 20$  keV, in reasonable agreement with this simple analytical estimate. As expected we observe that the crossover frequency increases with rising  $\tau$ , and asymptotically it should tend to infinity.

To check the precision of the calculations we test if the number density of the photons is conserved, as it should be in elastic Compton scattering. For  $T_e = 20$  keV and 1600 point grid in photon frequency the relative non-conservation of the photon number,  $\Delta N_\gamma/N_\gamma$ , is approximately  $10^{-9}$  for  $\tau = 0.01$  and is smaller than  $10^{-5}$  for any  $\tau < 20$ .

## 5. Conclusion

We have numerically calculated the spectral distortion of the cosmic background radiation produced by Compton scattering on hot electrons in galaxy clusters without any simplifying assumptions. We have analytically reduced the collision term in the Boltzmann equation to two dimensional integrals, and accurately solved the kinetic equation. Our analytical expression for the collision integral is exact, and can be used for any temperatures,  $T_\gamma$ ,  $T_e$ , and optical depth,  $\tau$ . The results are in good agreement with the previous works for small temperature and optical depth, but considerably different for large  $\tau$ . Our method can also be applied in the case of an isotropic electron distribution function, not necessarily in equilibrium.

We thank N. Itoh, Y. Kawana, S. Kusano, and S. Nozawa for sending us their program for the data fits from ref. Itoh et al. (2000a). A.D. is grateful to the Theory Division of CERN for the hospitality during the period when this work was completed. A.D., S.H. and S.P. are supported by INFN. In Munich, this work was partly supported by the Deutsche Forschungsgemeinschaft under grant No. SFB 375. The work of D.S. is supported in part by INTAS grant 1A-1065. S.P. is supported by the European Commission under the TMR network grant ERBFMRX-CT96-0090 and a Marie Curie fellowship under contract HPMFCT-2000-00445.

### A. Reduction of the collision integral

In this appendix we list the expressions for the 7 terms in the collision integral corresponding to the 7 terms in the matrix element eq. (10)

$$I_k(p_1) = \frac{\alpha^2}{2\pi p_1^2} \int_0^\infty \frac{p_2 dp_2}{E_2} \int_0^{\mathcal{S}} dp_3 F J_k(p_1, p_2, p_3). \quad (\text{A1})$$

The functions  $J_1, \dots, J_7$  depend upon the following combinations of the particle 3-momenta

$$\begin{aligned} \mathcal{P}^2 &\equiv (p_1 + E_2)^2 - m^2, & \mathcal{Q}^2 &\equiv (E_2 - p_3)^2 - m^2, \\ a &= \max(|p_1 - p_2|, |p_3 - p_4|), & b &= \min(p_1 + p_2, p_3 + p_4), \\ c &= \max(|p_1 - p_4|, |p_2 - p_3|), & d &= \min(p_1 + p_4, p_2 + p_3). \end{aligned} \quad (\text{A2})$$

In each case the value of  $p_4$  is obtained from the condition of energy conservation

$$p_1 + \sqrt{p_2^2 + m^2} = p_3 + \sqrt{p_4^2 + m^2}. \quad (\text{A3})$$

The integration over  $d^3 p_4$  and the angles of  $\mathbf{p}_2$  and  $\mathbf{p}_3$  with  $\delta$ -function imposing energy-momentum conservation is straightforward but rather lengthy, and we present only the final results

$$J_1 = m^4 \left[ \frac{1}{\mathcal{P}^3} \log \left| \frac{(\mathcal{P} + b)(\mathcal{P} - a)}{(\mathcal{P} - b)(\mathcal{P} + a)} \right| + \frac{2(b - a)(1 + ab/\mathcal{P}^2)}{(\mathcal{P}^2 - b^2)(\mathcal{P}^2 - a^2)} \right], \quad (\text{A4})$$

$$J_2 = -\frac{2m^2}{p_1 p_3}(d-c) = -\frac{2m^2}{p_1 p_3}(b-a), \quad (\text{A5})$$

$$J_4 = \frac{2m^2}{\mathcal{P}} \log \left| \frac{(\mathcal{P}+b)(\mathcal{P}-a)}{(\mathcal{P}-b)(\mathcal{P}+a)} \right|, \quad (\text{A6})$$

$$J_6 = \frac{b-a}{2} \left( 1 + \frac{(p_1^2 - p_2^2)(p_3^2 - p_4^2)}{\mathcal{P}^2 ab} \right) + \frac{m^2 p_1 p_3}{\mathcal{P}^3} \log \left| \frac{(\mathcal{P}+b)(\mathcal{P}-a)}{(\mathcal{P}-b)(\mathcal{P}+a)} \right|. \quad (\text{A7})$$

The explicit form of the other three  $J_i$  depends on the sign of  $Q^2$ . If  $Q^2 > 0$  then

$$J_3 = m^4 \left[ \frac{1}{Q^3} \log \left| \frac{(Q+d)(Q-c)}{(Q-d)(Q+c)} \right| + \frac{2(d-c)(1+cd/Q^2)}{(Q^2-d^2)(Q^2-c^2)} \right], \quad (\text{A8})$$

$$J_5 = \frac{2m^2}{Q} \log \left| \frac{(Q+d)(Q-c)}{(Q-d)(Q+c)} \right|, \quad (\text{A9})$$

$$J_7 = \frac{d-c}{2} \left( 1 + \frac{(p_1^2 - p_4^2)(p_3^2 - p_2^2)}{Q^2 cd} \right) + \frac{m^2 p_1 p_3}{Q^3} \log \left| \frac{(Q+d)(Q-c)}{(Q-d)(Q+c)} \right|, \quad (\text{A10})$$

while for the case  $Q^2 < 0$ , defining  $\mathcal{W}^2 = -Q^2$  we find

$$J_3 = 2m^4 \left[ \frac{1}{\mathcal{W}^3} \arctan \left( \frac{(d-c)\mathcal{W}}{\mathcal{W}^2 + cd} \right) + \frac{(d-c)(1+cd/Q^2)}{(Q^2-d^2)(Q^2-c^2)} \right], \quad (\text{A11})$$

$$J_5 = -\frac{4m^2}{\mathcal{W}} \arctan \left( \frac{(d-c)\mathcal{W}}{cd - Q^2} \right), \quad (\text{A12})$$

$$J_7 = \frac{d-c}{2} \left( 1 + \frac{(p_1^2 - p_4^2)(p_3^2 - p_2^2)}{Q^2 cd} \right) - \frac{2m^2 p_1 p_3}{Q^2 \mathcal{W}} \arctan \left( \frac{(d-c)\mathcal{W}}{cd - Q^2} \right). \quad (\text{A13})$$

## B. Integration region

In figs. 6 and 7 we present the integration region for the two-dimensional integral (A1), where we took the particular case  $p_1 = 1, m = 50 p_1$  and measure momenta  $p_i$  in units of  $p_1$ . The line  $p_3 = \mathcal{S} = p_1 + E_2 - m$  is the formal upper limit of integration over  $p_3$ , so  $0 \leq p_3 \leq \mathcal{S}$ . The integration region for  $p_2$  is  $0 < p_2 < \infty$ , but in fig. 7 we present it only for  $p_2 < m$ . Throughout the paper we consider the case of non-relativistic electrons,  $p_e \lesssim m$  but since we never expand in the electron mass, our analysis is valid for the general (relativistic) case.

We can cut away most of the integration region for  $p_3$  from the condition  $p_i \leq p_a + p_b + p_c$ , which follows from the momentum conservation, i.e. one momentum cannot be larger than the sum of all the others. For  $p_i = p_1$  or  $p_3$  this condition gives no reduction, but in case of  $p_i = p_2$  or  $p_4$  we cut regions  $E$  and  $F$  from the integration region<sup>5</sup> (see figs. 6 and 7). Thus only the regions  $A, B, C$  and  $D$  survive. To quantify this reduction let us note, that in the case of CMB distortion

---

<sup>5</sup>Note that region  $E$  only exists if  $p_1 < m/2$ .

in hot galaxy clusters one has  $p_e \sim \sqrt{2mT_e} \sim 100$  keV, while  $p_\gamma \sim 10^{-4}$  eV. In this case formally  $0 < p_3 < \mathcal{S} \sim 100$  eV, while non-zero contributions to the integrals in eq. (A1) come only from  $p_3 \sim 10^{-4}$  eV.

Figure 6 shows the integration region for relatively small momenta. One can see that besides the main integration regions  $C$  and  $D$  there are two small regions  $A$  and  $B$  which appear due to the fact that for a small momentum  $p_2$ , the condition  $p_2 = p_1 + p_3 + p_4$  is not operative, and the upper limit for  $p_3$  becomes  $p_3 = \mathcal{S}$ .

The regions  $A, B, C$  and  $D$  are defined in such a way, that in each of them our parameters  $a, b, c$  and  $d$  take definite values. This allows one to simplify the collision integral,  $I_{coll}$ , in each region. As we have seen in the previous section, there are generally two kinds of contribution to the collision integral, like  $J_1$  (which we will call  $\mathcal{P}$ -kind) and like  $J_3$  (which we will call  $\mathcal{Q}$ -kind). Fortunately the integration regions are identical for all integrals, and only the limits  $a, b, c$  and  $d$  will differ for the two kinds. For  $\mathcal{Q}$ -kind integrals we must distinguish between positive and negative  $\mathcal{Q}^2$  in the regions  $C$  and  $D$  (because  $\mathcal{Q}^2$  is always negative in regions  $A$  and  $B$ ). Therefore we introduce the regions  $C_1$  and  $D_1$  for  $\mathcal{Q}^2 < 0$ , and  $C_2$  and  $D_2$  regions for  $\mathcal{Q}^2 > 0$ . We have also separated the contribution from the  $\mathcal{Q}^2 = 0$  case, but this one-dimensional integral gives negligible contribution to the two-dimensional collision integral. Below we define each of the regions in detail.

### Region A.

$$0 < p_2 < p_1 \ ; \ p_1 < p_3 < p_1 + E_2 - m ,$$

and

- If  $p_1 < m/2$  then,

$$p_1 < p_2 < p_{change} \ ; \ \frac{p_1(E_2 + p_2)}{2p_1 - p_2 + E_2} < p_3 < p_1 + E_2 - m ,$$

where  $p_{change} = 2p_1(m - p_1)/(m - 2p_1)$  is the point in which  $p_2 = p_1 + p_3$  and  $p_4 = 0$ .

- If  $p_1 \geq m/2$  then,

$$p_1 < p_2 < \infty \ ; \ \frac{p_1(E_2 + p_2)}{2p_1 - p_2 + E_2} < p_3 < p_1 + E_2 - m ,$$

and region  $E$  does not exist.

In region  $A$  we have

$$a = p_3 - p_4 \ ; \ b = p_3 + p_4 \ ; \ c = p_1 - p_4 \ ; \ d = p_1 + p_4 .$$

### Region B.

$$0 < p_2 < p_1 \ ; \ \frac{p_1(E_2 + p_2)}{2p_1 - p_2 + E_2} < p_3 < p_1 .$$

In this region we have

$$a = p_1 - p_2 \ ; \ b = p_1 + p_2 \ ; \ c = p_3 - p_2 \ ; \ d = p_2 + p_3 .$$

### Region C<sub>1</sub>.

In this region  $Q^2 < 0$ . It is defined as

$$0 < p_2 < \min(p_1, p_{C_1}) \ ; \ \frac{p_1(E_2 - p_2)}{2p_1 + p_2 + E_2} < p_3 < \frac{p_1(E_2 + p_2)}{2p_1 - p_2 + E_2} ,$$

and

- If  $p_1 < m/2$  then,

$$p_1 < p_2 < p_{C_1} \ ; \ \frac{p_1(E_2 - p_2)}{2p_1 + p_2 + E_2} < p_3 < p_1 ,$$

- If  $p_1 \geq m/2$  then,

$$p_{C_1} < p_2 < p_1 \ ; \ E_2 - m < p_3 < \frac{p_1(E_2 + p_2)}{2p_1 - p_2 + E_2} ,$$

and

$$\max(p_1, p_{C_1}) < p_2 < p_{C_2} \ ; \ E_2 - m < p_3 < p_1 ,$$

where

$$p_{C_1} = \begin{cases} \frac{(m-2p_1)\sqrt{p_1(2m+p_1)}-2p_1(m-p_1)}{m-4p_1} & p_1 \neq \frac{m}{4} \\ \frac{5}{12}m & p_1 = \frac{m}{4} , \end{cases} \quad (\text{B1})$$

is the point, in which the line  $Q^2 = 0$  crosses the line  $p_4 = p_1 + p_2 + p_3$  (see figures 6 and 7). Let us just note the limiting cases for  $p_{C_1}$

$$\begin{aligned} p_1 \ll m & \quad p_{C_1} \rightarrow \sqrt{2p_1 m} , \\ p_1 = \frac{m}{2} & \quad p_{C_1} = p_1 = \frac{m}{2} , \\ p_1 \rightarrow \infty & \quad p_{C_1} = \frac{3}{4}m . \end{aligned} \quad (\text{B2})$$

The point in which the line  $Q^2 = 0$  crosses the line  $p_3 = p_1$  is

$$p_{C_2} = \sqrt{p_1(2m + p_1)} . \quad (\text{B3})$$

In region  $C_1$  we have

$$a = p_4 - p_3 \ ; \ b = p_1 + p_2 \ ; \ c = p_4 - p_1 \ ; \ d = p_2 + p_3 .$$

### Region $C_2$ .

In this region  $Q^2 > 0$ . It is defined as

$$p_{C_2} < p_2 < p_{C_2} \ ; \ \frac{p_1(E_2 - p_2)}{2p_1 + p_2 + E_2} < p_3 < E_2 - m ,$$

and

$$p_{C_2} < p_2 < \infty \ ; \ \frac{p_1(E_2 - p_2)}{2p_1 + p_2 + E_2} < p_3 < p_1 .$$

The limits  $a$ ,  $b$ ,  $c$  and  $d$  are the same as in region  $C_1$ .

### Region $D_1$ .

In this region  $Q^2 < 0$ . It is defined as

$$p_1 < p_2 < p_{C_2} \ ; \ p_1 < p_3 < \frac{p_1(E_2 + p_2)}{2p_1 - p_2 + E_2} ,$$

and

$$p_{C_2} < p_2 < p_D \ ; \ E_2 - m < p_3 < \frac{p_1(E_2 + p_2)}{2p_1 - p_2 + E_2} ,$$

where  $p_D$  is the point where the  $Q^2 = 0$  line crosses the line  $p_2 = p_1 + p_3 + p_4$ . This point is defined as

$$p_D = \begin{cases} \frac{(m-2p_1)\sqrt{p_1(2m+p_1)+2p_1(m-p_1)}}{m-4p_1} & p_1 < \frac{m}{4} \\ 3m/(4\epsilon) & p_1 = \frac{m}{4} - m\epsilon, \quad \epsilon \ll 1 \\ \infty & p_1 \geq m/4. \end{cases} \quad (\text{B4})$$

In region  $D_1$  we have

$$a = p_2 - p_1 \ ; \ b = p_3 + p_4 \ ; \ c = p_2 - p_3 \ ; \ d = p_1 + p_4 .$$

### Region $D_2$ .

In this region  $Q^2 > 0$ . It is defined as

$$p_{C_2} < p_2 < p_D \ ; \ p_1 < p_3 < E_2 - m ,$$

and if  $p_D$  is finite

$$p_D < p_2 < \infty \ ; \ p_1 < p_3 < \frac{p_1(E_2 + p_2)}{2p_1 - p_2 + E_2}.$$

The limits  $a$ ,  $b$ ,  $c$  and  $d$  are the same as in  $D_1$ .

## REFERENCES

- Bernstein, J. & Dodelson, S. 1990, Phys. Rev. D, 41, 354
- Birkinshaw, M. 1999a, Phys. Rep., 310, 97
- Birkinshaw, M. 1999b, in Proceedings of the EC-TMR Conference on 3K Cosmology, ed. L. Maiani, F. Melchiorri, & N. Vittorio (Woodbury, N.Y. : American Institute of Physics), 298
- Challinor, A. & Lasenby, A. 1998, ApJ, 499, 1
- Dolgov, A. D., Hansen, S. H., & Semikoz, D. V. 1997, Nucl. Phys. B, 503, 426
- Dolgov, A. D., Hansen, S. H., & Semikoz, D. V. 1998, Nucl. Phys. B, 524, 621
- Dolgov, A. D., Hansen, S. H., & Semikoz, D. V. 1999a, Nucl. Phys. B, 543, 269
- Dolgov, A. D., Hansen, S. H., Pastor, S., & Semikoz, D. V. 1999b, Nucl. Phys. B, 548, 385
- Hu, W. & Silk, J. 1993, Phys. Rev. D, 48, 485
- Itoh, N., Kohyama, Y., & Nozawa, S. 1998, ApJ, 502, 7
- Itoh, N., Kohyama, Y., & Nozawa, S. 2000a, ApJ, 536, 31
- Itoh, N., Kawana, Y., Nozawa, S., & Kohyama, Y. 2000b, preprint (astro-ph/0005390)
- Kompaneets, A. S. 1957, JETP Lett., 4, 730
- Lightman, A. P. 1981, ApJ, 244, 392
- Mather, J. C. et al. 1999, ApJ, 512, 511
- Molnar, S. M. & Birkinshaw, M. 1999, ApJ, 523, 78
- Nagirner, D. I. & Poutanen, J. 1994, Astrophys. Space Phys. Rev., 9, 1
- Poutanen, J. & Svensson, R. 1996, ApJ, 470, 249
- Press, W. H. et al. 1992, Numerical Recipes in C: the art of scientific computing (Cambridge: Cambridge Univ. Press)
- Raffelt, G. G. 1996, Stars as laboratories for fundamental physics (Chicago: Univ. of Chicago Press)



- Rephaeli, Y. 1995a, *ARA&A*, 33, 541
- Rephaeli, Y. 1995b, *ApJ*, 445, 33
- Rephaeli, Y. 1999, in *Proceedings of the EC-TMR Conference on 3K Cosmology*, ed. L. Maiani, F. Melchiorri, & N. Vittorio (Woodbury, N.Y. : American Institute of Physics), 310
- Rephaeli, Y. & Yankovitch, D. 1997, *ApJ*, 481, L55
- Sazonov, S. Y. & Sunyaev, R. A. 1998, *ApJ*, 508, 1
- Semikoz, D. V. & Tkachev, I. I. 1995, *Phys. Rev. Lett.*, 74, 3093
- Semikoz, D. V. & Tkachev, I. I. 1997, *Phys. Rev. D*, 55, 489
- Stebbins, A. 1997, preprint (astro-ph/9709065)
- Sunyaev, R. A. & Zeldovich, Ya. B. 1970a, *Ap&SS*, 7, 20
- Sunyaev, R. A. & Zeldovich, Ya. B. 1970b, *Comments Astrophys. Space Phys.*, , 2, 660
- Sunyaev, R. A. & Zeldovich, Ya. B. 1981, *Astrophys. Space Phys. Rev.*, 1, 1
- Wright, E. L. 1979, *ApJ*, 232, 348
- Zeldovich, Ya. B. & Novikov, I. D. 1983, *The structure & Evolution of the Universe* (Chicago & London: Univ. of Chicago Press)
- Zeldovich, Ya. B. & Sunyaev, R. A. 1969a, *ApJ*, 46, 775
- Zeldovich, Ya. B. & Sunyaev, R. A. 1969b, *Ap&SS*, 4, 301

Fig. 1.— First-order contribution to the spectral distortion of photons for  $T_e = 10$  keV and  $T_e = 20$  keV as a function of the dimensionless photon frequency  $X$ . Our numerical results are presented by the solid and dashed lines, whereas the data points correspond to the analytical fit from Itoh et al. (2000a).

Fig. 2.— Second-order contribution to the spectral distortion of photons for  $T_e = 10$  keV as a function of the dimensionless photon frequency  $X$ . Our numerical result are presented by the solid line, whereas the dashed, short dashed and dotted lines correspond to the series expansion from Itoh et al. (2000b).

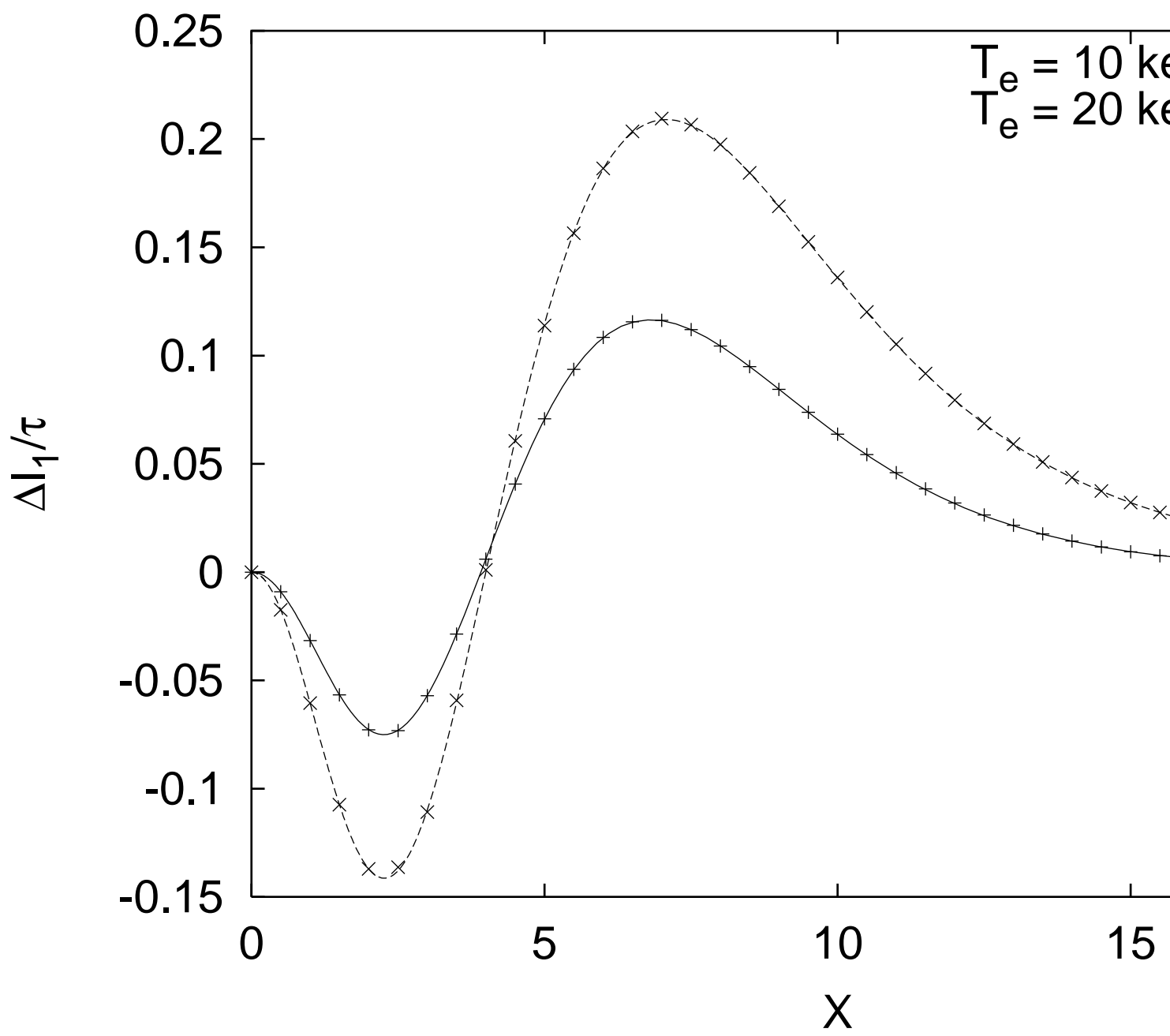
Fig. 3.— Spectral distortion of photons for optical depth  $\tau = 1$  and  $T_e = 20$  keV as a function of the dimensionless photon frequency  $X$ .

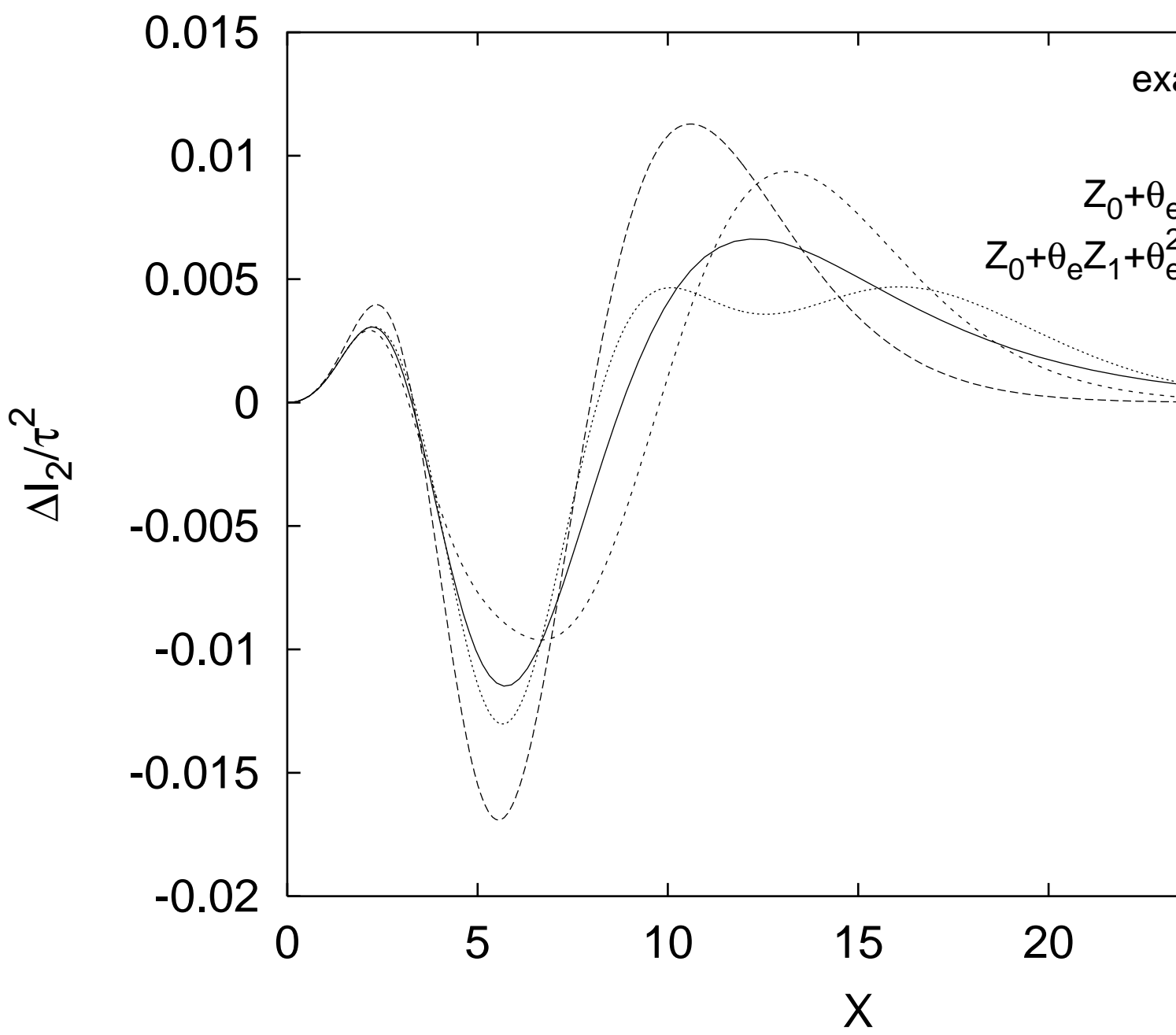
Fig. 4.— Crossover frequency  $X_0$  as a function of the electron temperature  $T_e$  for  $\tau = 0.01$  and the regions, where double photon scattering gives a contribution to the spectral distortion larger than 1% (long dashed lines), 10% (short dashed lines), and 50% (dotted lines) respectively.

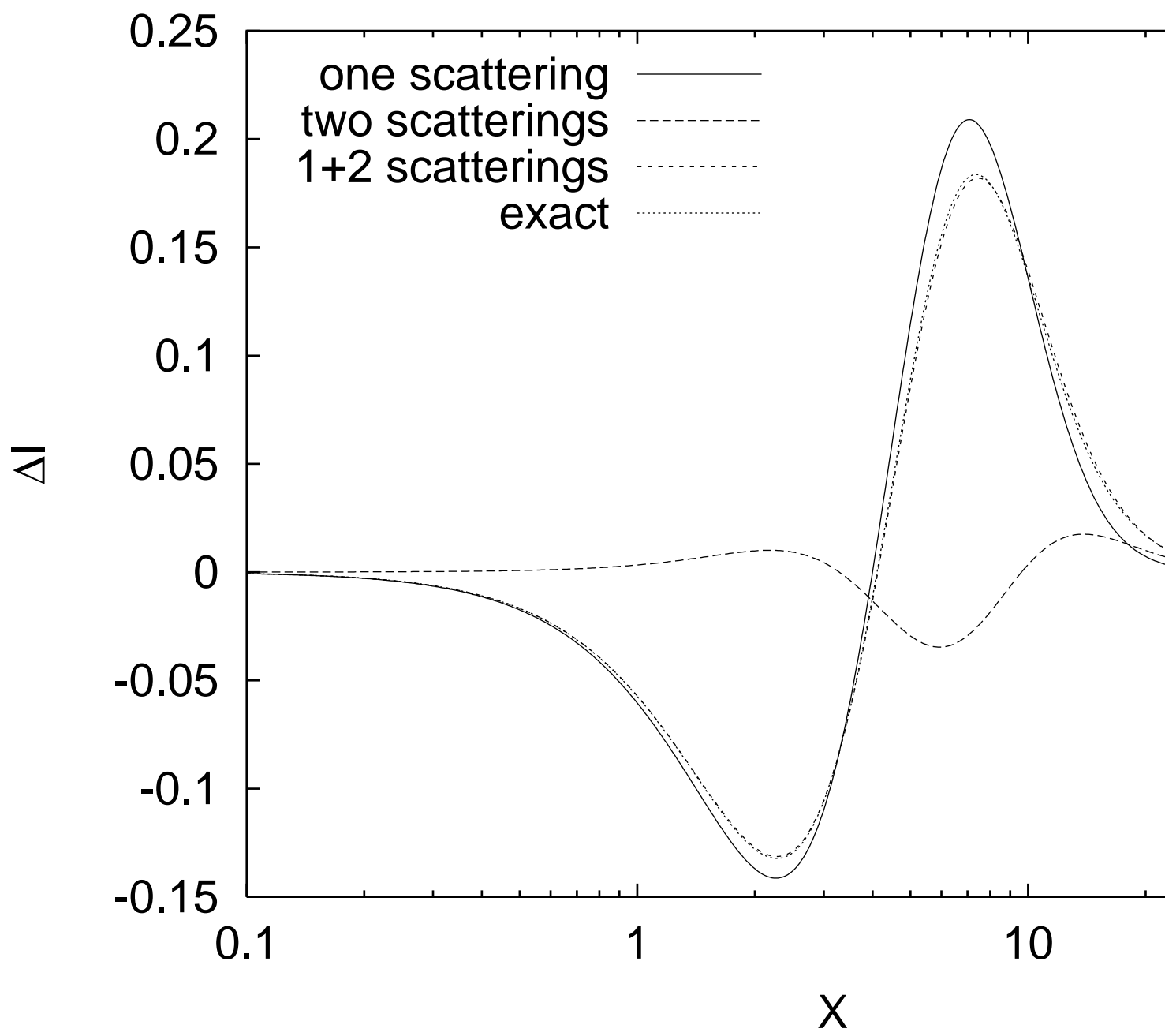
Fig. 5.— Spectral distortion of photons for  $T_e = 20$  keV as a function of the dimensionless photon frequency  $X$  for several optical depths up to  $\tau = 20$ .

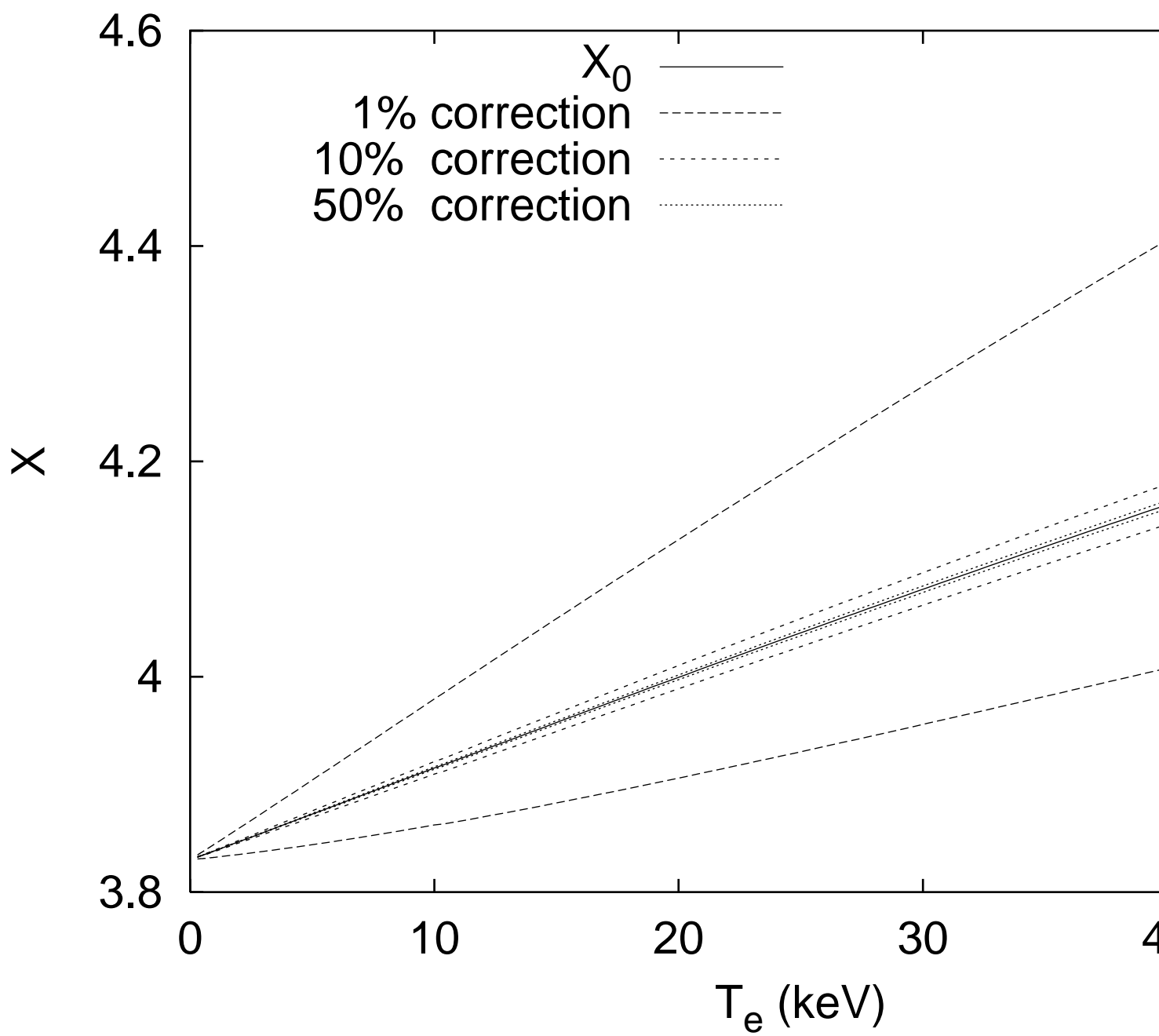
Fig. 6.— Region of integration of two-dimensional integral for small momenta.

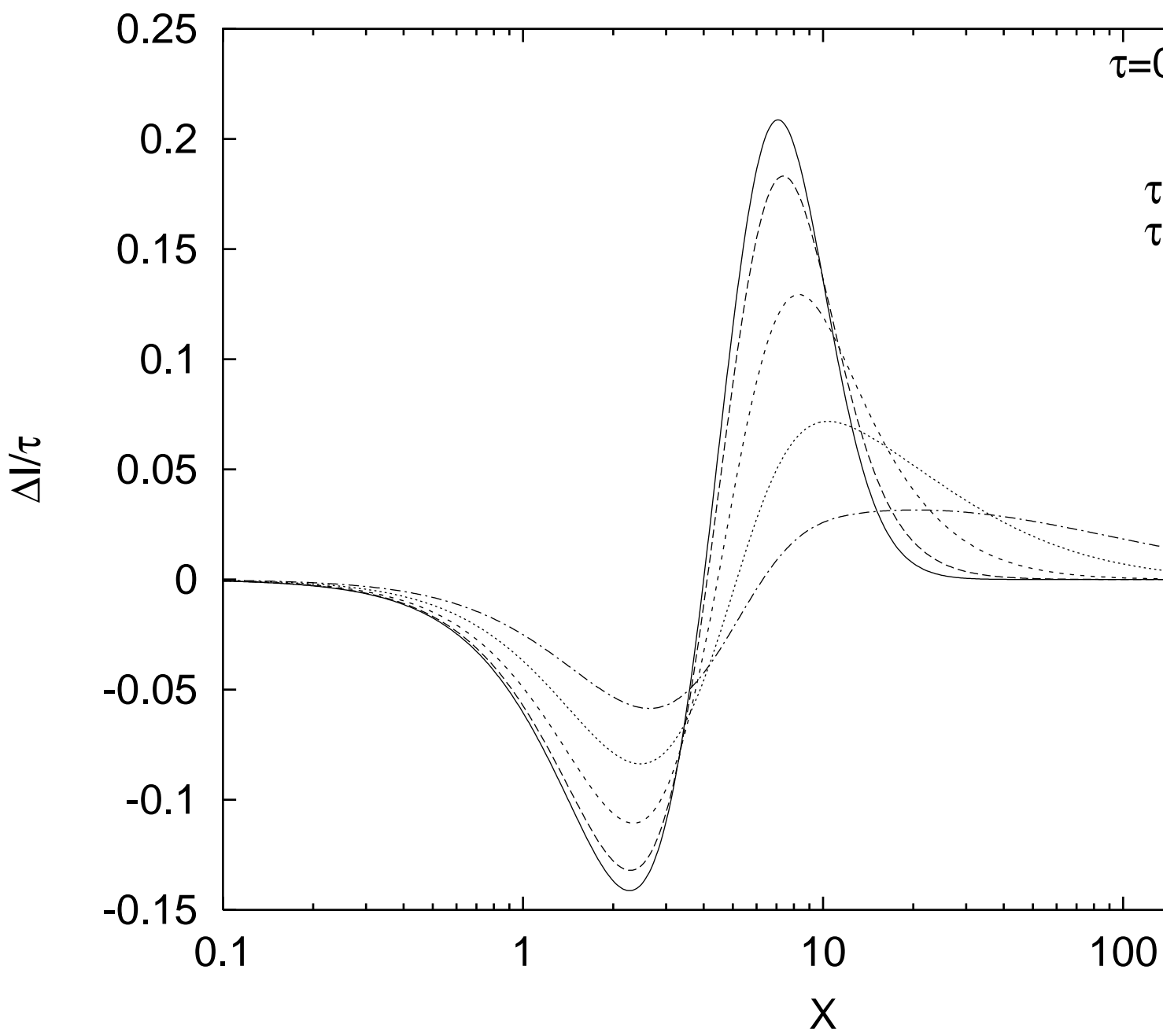
Fig. 7.— Region of integration of two-dimensional integral.











$m_e=50, p_1=1$

$p_4=p_1+p_2$   
 $p_3=p_1+E_2$   
 $p_2=p_1+p_3$   
 $p_1+p_3=p_2$   
 $p_3=$

